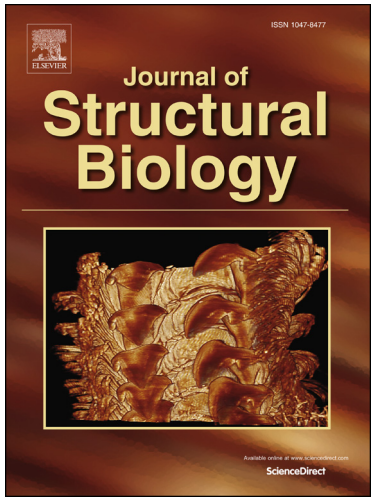

Technical note

An improved cryo-FIB method for fabrication of frozen hydrated lamella

Jianguo Zhang, Gang Ji, Xiaojun Huang, Wei Xu, Fei Sun

PII: S1047-8477(16)30028-4
DOI: http://dx.doi.org/10.1016/j.jsb.2016.02.013
Reference: YJSBI 6862

To appear in: *Journal of Structural Biology*

Received Date: 18 November 2015
Revised Date: 2 January 2016
Accepted Date: 11 February 2016

Please cite this article as: Zhang, J., Ji, G., Huang, X., Xu, W., Sun, F., An improved cryo-FIB method for fabrication of frozen hydrated lamella, *Journal of Structural Biology* (2016), doi: http://dx.doi.org/10.1016/j.jsb.2016.02.013

An improved cryo-FIB method for fabrication of frozen hydrated lamella

Jianguo Zhang [1, #], Gang Ji [1, #], Xiaojun Huang [1], Wei Xu [1, *], Fei Sun [1, 2, 3, *]

[1] Center for Biological Imaging, Institute of Biophysics, Chinese Academy of Sciences, 15 Datun Road, Beijing 100101, China.

[2] National Laboratory of Biomacromolecules, Institute of Biophysics, Chinese Academy of Sciences, 15 Datun Road, Beijing 100101, China.

[3] University of Chinese Academy of Sciences, Beijing, China.

[#] These authors make equal contributions to this work.

* Correspondence: emlb@ibp.ac.cn (Wei Xu) or feisun@sun5.ibp.ac.cn (Fei Sun)

Running Title: cryo-FIB fabricating frozen hydrated lamella

ABSTRACT

Cryo-electron tomography (cryo-ET) provides great insights into the ultrastructure of cells and tissues in their native state and provides a promising way to study the in-situ 3D structures of macromolecular complexes. However, this technique has been limited on the very thin specimen, which is not applicable for most cells and tissues. Besides cryo-sectioning approach, cryo focused ion beam (cryo-FIB) appeared recently to achieve 'artifact-free' thin frozen hydrated lamella via fabrication. Considering that the current cryo-FIB methods need modified holders or cartridges, here, with a "D-shaped" molybdenum grid and a specific shutter system, we developed a simple cryo-FIB approach for thin frozen hydrated lamella fabrication, which fits both standard transmission cryo-electron microscopes with side-entry cryo-holders and state-of-the-art ones with AutoGrids. Our approach will expand the usage of cryo-FIB approach in many labs.

KEY WORDS: Cell ultrastructure; Cryo-electron tomography; Cryo-focused ion beam; Frozen hydrated lamella; Molybdenum grid.

1. Introduction

Cryo-electron tomography (cryo-ET) is an important approach to study the cell ultrastructure in its near native state, providing fruitful information for structural biology and cell biology studies (Fridman et al., 2012; Lucic et al., 2013; Rigort et al., 2012a; Yahav et al., 2011). In the past decades, cryo-ET has been successfully applied in the structural studies of several bacterial cells and small eukaryotic cells at their edges (Cyrklaff et al., 2007; Maurer et al., 2008). However, the application of cryo-ET is also significantly restricted to the thickness of the specimen less than 500 nm while most eukaryotic cells and tissue samples are much thicker. The primary solution to thin the frozen-hydrated cells and tissues was developed for decades with the technique of cryo-section by cryo-ultramicrotomy (Al-Amoudi et al., 2004; Hsieh et al., 2006; McDowall et al., 1983). The term cryo-electron microscopy of vitreous sections (CEMOVIS) was also given for this technique, which normally includes the procedures of high pressure freezing, cryo-trimming and sectioning, and cryo-electron tomography. However, there are some unavoidable problems during cryo-sectioning, e.g. sample compression in the range of 30-50% along the cutting direction, knife marks, knife chatter, poor section adhesion, bending of sections and etc. These cutting artifacts by cryo-ultramicrotomy will cause severe problems for the followed data collection and image analysis of cryo-ET (Al-Amoudi et al., 2005;

Rigort et al., 2010), thus limiting the wide application of cryo-ET in structural biology and cell biology.

Recently, Mark et al. developed a technique of the cryo focused ion beam (cryo-FIB) milling and demonstrated that vitreous water could be thinned by this technique and no re-crystallized ice appears during milling (Marko et al., 2006). This technique was firstly applied on the structural studies of biological specimen, *E.coli* cells (Marko et al., 2007). Then this technique was further applied to study the structures of nuclear pore complexes (NPC) in the eukaryotic microbial cells (Rigort et al., 2012b) and study the 3D native ultrastructure of mammalian cells (Strunk et al., 2012; Wang et al., 2012). Furthermore, this technique was also incorporated into a workflow from cryo-preparation and then cryo-fluorescence microscopy to correlated cryo-ET for structural studies of cultured cells (Rigort et al., 2010). Besides cultured cells, cryo-FIB was also proved useful to thin *C.elegans*, a typical model for multicellular organism, which was high pressure frozen on EM grids (Harapin et al., 2015). In recent years, Mark et al further developed cryo-FIB technique by designing additional adapters for milling tissues (e.g. skeletal muscles) that were cryo-fixed by high-pressure freezing (Hsieh et al., 2014; Wagenknecht et al., 2015). Recently, Mahamid et al developed a cryo-micromanipulator tool to lift out the cryo-FIB milled frozen-hydrated lamella, which expanded the flexibility in the following cryo-fluorescence microscopy and

cryo-ET (Mahamid et al., 2015). With the recent progresses of cryo-FIB, we could foresee the great potential of this "artifact-free" technique for the future structural biology in-situ (Rigort and Plitzko, 2015).

However, to our best knowledge, most current cryo-FIB applications are in combination with high-end 300kV transmission electron microscopes and AutoGrids (Mahamid et al., 2015; Rigort et al., 2012b; Strunk et al., 2012; Wang et al., 2012) or with sophisticated devices (Hsieh et al., 2014; Rigort et al., 2010). Such situation limits the wide application of cryo-FIB technique in many labs. Here, using a "D-shaped" molybdenum grid and a specific shutter system, we developed a convenient cryo-FIB workflow that could be suitable for both the high-end cryo-transmission electron microscopes (cryo-TEM) with AutoGrids and the conventional microscopes with the standard side-entry cryo-holders (e.g. Gatan Model 626).

2. Sample preparation

2.1 Preparation of *E.coli* cells

E.coli cells were grown on LB broth (10% tryptone, 5% yeast extract and 10% NaCl) over night at 37 ℃ with the shaking speed of 280 rpm. When the culture was grown to an optical density of 2.0 at the wavelength of 600 nm, the cells were collected by centrifugation at 1,000 rpm for 5 min and the supernatant was discarded. The *E.coli* cells were then suspended in the PBS buffer containing

additional 0.5 g/L Mg^{2+} and washed twice before plunge freezing.

2.2 Preparation of *Ascaris Suum* sperm cells

Ascaris Suum sperm cells came from dissecting *Ascaris Suum*. The cells in the PBS buffer containing additional 0.5 g/L Mg^{2+} were collected by centrifugation at 2,000 rpm for 5min and the supernatant was discarded. The cells were then suspended in the PBS buffer containing additional 0.5 g/L Mg^{2+} and washed twice before plunge freezing.

2.3 Preparation of SF9 insect cells

The SF9 cells were cultured at 37 ℃ with 5% CO_2 and in the medium of DMEM with 10% FBS and 1% Penicillin-Streptomycin solution (100 x). The cultured cells were passaged by 0.25% Trypsin-EDTA for 2 min. Then the cells were collected by a cell scraper and suspended in the culture. The suspension solution was centrifuged at 3,000 rpm for 5 min and the supernatant was discarded. The pellet cells were then suspended in the PBS buffer containing additional 0.5 g/L Mg^{2+} and washed twice before plunge freezing.

2.4 Preparation of mouse embryonic fibroblasts (MEF) cells

The MEF cell lines were cultured in Dulbecco's modified Eagle's medium (Sigma) supplemented with 10% heat-inactivated fetal bovine serum (Gibco) and in a 5% CO_2 incubator at 37 ℃. After additional 48 hr incubation, the cells were

collected with a cell scraper and suspended in the culture. The suspension solution was centrifuged at 3,000 rpm for 5 min and the supernatant was discarded. The pellet cells were then suspended in the PBS buffer containing additional 0.5 g/L Mg^{2+} and washed twice before plunge freezing.

2.5 Plunge freezing of grids

Before applying the suspended cells, the grids were cleaned by the glow discharge for 10 s using the plasma cleaner (Harrick Plasma PDC-32G) with the medium FR lever. Then the grids were plunge-frozen into liquid ethane (close to liquid solid mixed state) that was cooled by liquid nitrogen by using FEI Vitrobot IV (FEI Corp., OR) with the blotting chamber temperature of 37 ℃, humidity of 100%, blot force of 4 and bolt time of 10 s. After plunge freezing, the grids were transferred to storage grid box (LifeTrust, Jiangsu, China) in the liquid nitrogen before cryo-FIB milling.

3. Design of cryo-transfer shutter system

In order to protect the vitrified specimen from frost contamination, to keep the vitrified temperature of the specimen and to help the multi-step cryo-transfer, we designed a transfer station (**Figure 1A**), a transfer shuttle (**Figure 1B**) and a special “D-shaped” grid (**Figures 1C**).

The shell of the transfer station consists of polystyrene material and

accommodates the liquid nitrogen reservoir. There are three positions designed for the placement of cryo-grid boxes, ensuring a smooth transfer of cryo-grids from the cryo-grid box into the cryo-transfer shuttle. The shuttle position is designed for fixing the shuttle that is ready to install or recover the cryo-grids. The hollow out platform is designed for storing liquid nitrogen at the bottom of the cup to keep the cryogenic temperature of the station (**Figure 1A**).

The transfer shutter is made with pure copper material (**Figure 1B)**. The cover of the shutter is kept close all the time, except FIB milling and grid transfer. The cover opening and closing process are operated using a freeze-fracture knife in the sample preparation chamber of Quorum PP3000T cryo-transfer system (Quorum Technologies, East Sussex, UK). The crosshead fixing screw is designed to lock the cover during the storage of the shutter after FIB milling in some cases. The cryo-condition of the shutter in the SEM (scanning electron microscope) chamber is kept by the cryo-stage of Quorum PP3000T cryo-transfer system (**Figure 1E**).

We designed a special 200-mesh “D-shaped” molybdenum grid with 1/4 portion trimmed (**Figure 1C**) for our cryo-FIB milling experiments. The molybdenum grids are mechanically hard with small expansion coefficient in the liquid nitrogen, which benefits the workflow of multi-step transfer in cryo-FIB experiments. The flat edge of the grid can keep the same direction of the grid between cryo-FIB milling

and cryo-TEM, which is important for the following cryo-ET data collection. In addition, such special designed grid can be loaded onto both the AutoGrid and the standard side-entry cryo-holder (**Figure 1D**). These special customized "D-shaped" molybdenum grids coated with lacey support film were bought from Beijing Xinxing Braim Technology.

4. Cryo-FIB fabrication and cryo-electron microscopy

Cryo-FIB milling experiments were performed using Helios NanoLab 600i Dual Beam SEM (FEI, Netherlands) with a field emission electron source, gallium ion source and the in-lens electron detector. The frozen grids were transferred with the cryo-transfer shuttle into the SEM chamber by using Quorum PP3000T cryo-transfer system (Quorum Technologies, East Sussex, UK) under -180 ℃.

During the cryo-FIB milling process, it is important to keep the milling angle as small as possible, because the smaller angle can fabricate a larger view region and therefore the thinned section is flat enough on the grid (Rigort et al., 2010; Wang et al., 2012). In this experiment, the milling angel between the FIB and the specimen surface was set to 10°~15°. The milling was performed parallel from two sides to produce vitrified cell lamella (Rigort et al., 2010). The accelerating voltage of the ion beam was kept 30 kV, and the ion currents were in the range from 0.23 nA to 80 pA. The rough milling utilized a strong ion beam current of 0.23 nA and the final fine milling was operated with a small ion beam current of 80 pA.

The thickness of the residual thin lamella with a good quality is about 200~300 nm.

After cryo-FIB milling, the cryo-grid was transferred into the cryo-grid box from the transfer shutter by using the transfer station. Then the cryo-grid was further transferred into the standard side-entry cryo-holder or the AutoGrid for cryo-electron microscopy.

For transferring into the standard cryo-holder (here, Gatan Model 626), with the special “D” shape, the grid is easy to mount onto the holder with a right direction. After grid loading, the cryo-holder was inserted into a FEI Tecnai 20 transmission electron microscope that is operated in 200 kV and equipped with a Gatan Ultrascan 1000 CCD camera (2048*2048 pixels). Tilt series were collected in low-dose condition automatically using SerialEM (Mastronarde, 2005) with the tilt angle from -60° to 60° and the angle increment of 2°. The total dose used is 12,000 e/nm and the nominal magnification is 11,500 with the actual pixel size of 1.32 nm/pixel. The images were recorded with the averaged defocus value of ~ 10 μm.

For transferring into the AutoGrid, the easily recognized grid shape also provides benefits for mounting AutoGrid into the cassette with a right direction. FEI Titan Krios transmission electron microscope was used to collect cryo-electron tomography data of specimen in the AutoGrid. The microscope is

operated in 300 kV and equipped with a FEI Falcon II camera (4096×4096 pixels). Tilt series were collected in low-dose condition automatically using SerialEM (Mastronarde, 2005) with the tilt angle from -60° to 60° and the angle increment of 2°. The total dose used is 100 e/Å^2 and the nominal magnification is 29,000 with the actual pixel size of 0.29 nm/pixel. The images were recorded with the averaged defocus value of ~10 μm.

All the collected tilt series were aligned, reconstructed and post-processed by IMOD software (Kremer et al., 1996).

4.1 Cryo-FIB milling of *E.coli* cells and *Ascaris Suum* sperm cells

The first test was performed on *E.coli* cells, the typical small sized cells. Normally, there are 3~5 regions milled by cryo-FIB and these regions can be viewed from low magnification SEM image (secondary electron signal, see **Figure 2A**). And the cryo-hydrated lamella can be recognized from a high magnification SEM image (**Figure 2B**). The thickness of the section can be estimated as ~ 377 nm from the FIB direction (FIB induced secondary electron signal, see **Figure 2C**). The followed low-dose cryo-TEM images of the cryo-FIB milled lamella showed that the section of *E.coli* cells are preserved in the vitreous state with no obvious radiation damage after cryo-FIB milling (**Figure 2D**) and the inner- and outer-membranes structure of the cell are clearly resolved in cryo-TEM (**Figure 2E**).

Another test was performed on *Ascaris Suum* sperm cells, another type of

small sized cells (**Figures 2F, 2G and 2H**). Some occasional ice crystal contamination on the cryo-FIB milled lamella can be observed by the low magnification TEM image (**Figure 2F**) and we speculate that such contamination comes from the specimen transfer procedure. The size of the cryo-FIB milled lamella is about 20*8 μm, which is sufficient for the following cryo-TEM and cryo-ET data collection. From this cryo-FIB milled lamella of *Ascaris Suum* sperm cell, many cytoplasmic ultrastructures can be clearly observed by low-dose cryo-TEM, e.g. the reflector body (RB), vesicles (V) and other membrane organelles (**Figures 2G and 2H**).

4.2 Cryo-FIB milling of the insect SF9 cells and cryo-ET using the side-entry cryo-holder

Our cryo-FIB workflow was further tested to apply on bigger sized cells, the insect SF9 cells. A 200~400 nm lamella were prepared by cryo-FIB (**Figure 3A**). After examination in low magnification cryo-TEM (**Figure 3B**), a good region of the cryo-FIB milled lamella was selected for further investigation in high magnification (**Figure 3C**). Besides occasional large ice crystal contamination (**Figure 3B**), most parts of the lamella are clean and preserved in vitreous state with natural morphology of various organelles, e.g. mitochondria, vesicles, microtubules, ribosomes and etc. The region of interest was further selected for tomographic data collection by using a standard side-entry cryo-holder (Gatan

Model 626) and an FEI Tecnai 20 transmission electron microscope. After the tomographic reconstruction, the abundant 3D structural details of the insect SF9 cell at the cytoplasmic region were clearly resolved from the tomogram, including double membrane of mitochondria, mitochondrial cristae, ribosomes, microtubules and etc. (**Figure 3D and Movie S1**).

4.3 Cryo-FIB milling of MEF cells and cryo-ET using the AutoGrid

Another cryo-FIB workflow test was performed to prepare cryo-hydrated lamella of MEF cells, which was loaded onto the AutoGrid and imaged by FEI Titan Krios (FEI Corp., Netherland). The orientation of the cryo-grid was well controlled with the special grid edge during the whole transferring and loading procedure. The quality of the cryo-FIB milled lamella was examined as above and a region of interest was selected for tomographic data collection. From the tomogram, we observed abundant 3D structural details of MEF cell, including the fission of mitochondrion, the microfilaments at the mitochondrial fission site, microtubules around the mitochondrion, large vesicular organelles with many macromolecular complexes on the membrane and lots of ribosomes (**Figures 3E-H and Movie S2**). To our best knowledge, the structural moieties at the fission site of mitochondrion (Figures 3E and 3F) have never been observed before and would raise the future study for its biological significance.

Overall, the applications of our cryo-FIB approach on the bacterial cells, worm

sperm cells, insect cells and embryonic fibroblast cells demonstrate that our cryo-FIB workflow can fabricate high quality frozen-hydrated lamella of biological specimen for the high-resolution cryo-electron tomography studies.

ACKNOWLEDGEMENTS

The authors are grateful to Lianwan Chen, Shengliu Wang, Wei Zhao and Huiqin Luan for providing available cells. This work was supported by grants from the Strategic Priority Research Program of Chinese Academy of Sciences (XDB08030202) to FS, the National Basic Research Program (973 Program) of Ministry of Science and Technology of China (2014CB910700) to FS, National Natural Science Foundation of China (31470838) to GJ and National Natural Science Foundation of China (31400734) to JGZ. All the EM works were performed at Center for Biological Imaging (CBI, http://cbi.ibp.ac.cn), Institute of Biophysics, Chinese Academy of Sciences.

REFERENCES

Al-Amoudi, A., Studer, D., Dubochet, J., 2005. Cutting artefacts and cutting process in vitreous sections for cryo-electron microscopy. Journal of structural biology 150, 109-121.

Al-Amoudi, A., Chang, J.J., Leforestier, A., McDowall, A., Salamin, L.M., Norlen, L.P., Richter, K., Blanc, N.S., Studer, D., Dubochet, J., 2004. Cryo-electron microscopy of vitreous sections. The EMBO journal 23, 3583-3588.

Cyrklaff, M., Linaroudis, A., Boicu, M., Chlanda, P., Baumeister, W., Griffiths, G., Krijnse-Locker, J., 2007. Whole cell cryo-electron tomography reveals distinct disassembly intermediates of vaccinia virus. PLoS One 2, e420.

Fridman, K., Mader, A., Zwerger, M., Elia, N., Medalia, O., 2012. Advances in tomography: probing the molecular architecture of cells. Nat Rev Mol Cell Biol 13, 736-742.

Harapin, J., Bormel, M., Sapra, K.T., Brunner, D., Kaech, A., Medalia, O., 2015. Structural analysis of multicellular organisms with cryo-electron tomography. Nature methods 12, 634-636.

Hsieh, C., Schmelzer, T., Kishchenko, G., Wagenknecht, T., Marko, M., 2014. Practical workflow for cryo focused-ion-beam milling of tissues and cells for cryo-TEM tomography. Journal of structural biology 185, 32-41.

Hsieh, C.E., Leith, A., Mannella, C.A., Frank, J., Marko, M., 2006. Towards high-resolution three-dimensional imaging of native mammalian tissue: electron tomography of frozen-hydrated rat liver sections. J Struct Biol 153, 1-13.

Kremer, J.R., Mastronarde, D.N., McIntosh, J.R., 1996. Computer visualization of three-dimensional image

data using IMOD. Journal of Structural Biology 116, 71-76.

Lucic, V., Rigort, A., Baumeister, W., 2013. Cryo-electron tomography: the challenge of doing structural biology in situ. J Cell Biol 202, 407-419.

Mahamid, J., Schampers, R., Persoon, H., Hyman, A.A., Baumeister, W., Plitzko, J.M., 2015. A focused ion beam milling and lift-out approach for site-specific preparation of frozen-hydrated lamellas from multicellular organisms. Journal of structural biology.

Marko, M., Hsieh, C., Moberlychan, W., Mannella, C.A., Frank, J., 2006. Focused ion beam milling of vitreous water: prospects for an alternative to cryo-ultramicrotomy of frozen-hydrated biological samples. J Microsc 222, 42-47.

Marko, M., Hsieh, C., Schalek, R., Frank, J., Mannella, C., 2007. Focused-ion-beam thinning of frozen-hydrated biological specimens for cryo-electron microscopy. Nat Methods 4, 215-217.

Mastronarde, D.N., 2005. Automated electron microscope tomography using robust prediction of specimen movements. J Struct Biol 152, 36-51.

Maurer, U.E., Sodeik, B., Grunewald, K., 2008. Native 3D intermediates of membrane fusion in herpes simplex virus 1 entry. Proc Natl Acad Sci U S A 105, 10559-10564.

McDowall, A.W., Chang, J.J., Freeman, R., Lepault, J., Walter, C.A., Dubochet, J., 1983. Electron microscopy of frozen hydrated sections of vitreous ice and vitrified biological samples. Journal of microscopy 131, 1-9.

Rigort, A., Plitzko, J.M., 2015. Cryo-focused-ion-beam applications in structural biology. Arch Biochem Biophys 581, 122-130.

Rigort, A., Villa, E., Bauerlein, F.J., Engel, B.D., Plitzko, J.M., 2012a. Integrative approaches for cellular cryo-electron tomography: correlative imaging and focused ion beam micromachining. Methods Cell Biol 111, 259-281.

Rigort, A., Bauerlein, F.J., Villa, E., Eibauer, M., Laugks, T., Baumeister, W., Plitzko, J.M., 2012b. Focused ion beam micromachining of eukaryotic cells for cryoelectron tomography. Proc Natl Acad Sci U S A 109, 4449-4454.

Rigort, A., Bauerlein, F.J., Leis, A., Gruska, M., Hoffmann, C., Laugks, T., Bohm, U., Eibauer, M., Gnaegi, H., Baumeister, W., Plitzko, J.M., 2010. Micromachining tools and correlative approaches for cellular cryo-electron tomography. Journal of structural biology 172, 169-179.

Strunk, K.M., Wang, K., Ke, D., Gray, J.L., Zhang, P., 2012. Thinning of large mammalian cells for cryo-TEM characterization by cryo-FIB milling. Journal of microscopy 247, 220-227.

Wagenknecht, T., Hsieh, C., Marko, M., 2015. Skeletal muscle triad junction ultrastructure by Focused-Ion-Beam milling of muscle and Cryo-Electron Tomography. Eur J Transl Myol 25, 49-56.

Wang, K., Strunk, K., Zhao, G., Gray, J.L., Zhang, P., 2012. 3D structure determination of native mammalian cells using cryo-FIB and cryo-electron tomography. J Struct Biol 180, 318-326.

Yahav, T., Maimon, T., Grossman, E., Dahan, I., Medalia, O., 2011. Cryo-electron tomography: gaining insight into cellular processes by structural approaches. Curr Opin Struct Biol 21, 670-677.

FIGURE LEGENDS

Figure 1. **Design of the cryo-FIB transfer station, the transfer shuttle and the "D"-shaped grid.** (**A**) The drawing of the cryo-FIB transfer station. (**B**) The drawing of the cryo-FIB transfer shuttle with the specimen protection cover close (left) and open (right), respectively. The angle between the grid-loading slot and the horizontal plane is 30°. The crosshead fixing screw shown left is used during the storage of the shutter in the liquid nitrogen. (**C**) The design of a "D"-shaped molybdenum grid with one quarter trimmed and regions labeled. (**D**) The grids mounted onto the AutoGrid (left) and the standard side-entry cryo-holder (right). (**E**) A snapshot of the SEM (FEI Helios Nanolab 600i Dual Beam) chamber with the cryo-FIB transfer shuttle mounted onto the Quorum PP3000T cryo-stage.

Figure 2. **Cryo-FIB milling of frozen-hydrated *E. coli* and *Ascaris Suum* sperm cells.** (**A**) Cryo-scanning electron micrograph (secondary electron signal) of vitrified *E. coli* cells on an EM grid after cryo-FIB milling. (**B**) Magnified view of the milled region in (A). (**C**) Vertical view of the milled region from the FIB direction, which is imaged using the signal of FIB-induced secondary electrons. (**D**) and (**E**) Low-dose cryo-TEM micrographs of cryo-FIB milled *E.coli* cells. The region in the white dashed window is zoomed in at the corner. (**F**), (**G**) and (**H**) Low-dose cryo-TEM micrographs of cryo-FIB milled *Ascaris Suum* sperm cell lamella at the low (F), medium (G) and high magnification (H) respectively. TEM imaging was

taken by using FEI Tecnai 20 microscope. Some frost particles can be discerned across the lamella as indicated with the white asterisk. Scale bars: (A) 100μm, (B) 50 μm, (C) 10μm, (D) 500nm, (E) 300nm, (F) 10μm, (G) 2μm and (H) 1μm.

Figure 3. **Cryo-FIB milling and cryo-ET of frozen-hydrated insect SF9 cells and MEF cells**. (**A**) Low-dose cryo-TEM images of cryo-FIB milled insect SF9 cell lamella. (**B**) Middle magnification of the selected region in (A). Some frost particles can be discerned across the lamella as indicated with the white asterisks. (**C**) High magnification of the selected region in (B). (**D**) Tomographic reconstruction of the cryo-FIB milled insect SF9 cell lamella at the region in (C). The microtubules are indicated with the black arrows. TEM imaging was taken by using FEI Tecnai 20 microscope. (**E**), (**F**), (**G**) and (**H**) the z-slices of tomogram of the cryo-FIB milled MEF cell lamella with different z-positions. The traversing microtubules (MT) and microfilaments (MF) are indicated with the arrowheads. TEM imaging was taken by using FEI Titan Krios microscope. Scale bars: (A) 1 μm (B) 500 nm, (C) 400 nm and (D) 300 nm, and (E) 200 nm.

SUPPLEMENTAL MOVIE LEGENDS

Movie S1. Slicing view of tomogram of cryo-FIB milled insect SF9 cell lamella.

Movie S2. Slicing view of tomogram of cryo-FIB milled MEF cell lamella.